

The system $\text{SiO}_2\text{--H}_2\text{O--CO}_2$: melting, solubility mechanisms of carbon, and liquid structure to high pressures¹

A. L. BOETTCHER

*Institute of Geophysics and Planetary Physics
and Department of Earth and Space Sciences
University of California, Los Angeles
Los Angeles, California 90024*

Abstract

To serve as a model for the solubility mechanisms of carbon in silicate liquids and as a model for melting relationships in systems containing multi-component vapors, the system $\text{SiO}_2\text{--H}_2\text{O--CO}_2$ was investigated to pressures of 27.5 kbar and temperatures from 1000 to 1650°C. The solubility of carbon in the hydrous liquids increases markedly above 10–15 kbar, probably entering the liquid as molecular CO_2 , possibly in part as tetrahedral carbon. Phase transformations in the high-pressure liquids, such as quartz \rightleftharpoons coesite structure, may enhance the solubility. The amount of carbon in solution is unknown, particularly at the lower pressures, and this precludes calculation of the activity coefficients of H_2O in the $\text{H}_2\text{O--CO}_2$ vapors. The solubility mechanisms and data on the liquids in this system may also apply to the more complex, aluminosilicate magmas.

Introduction

Throughout the last decade, there have been numerous studies of mixed volatile components in silicate systems at high pressures to assess their effect on melting relationships in rock systems (e.g., Wyllie, 1979; Mysen and Boettcher, 1975) and to determine thermodynamic properties of multicomponent fluids (e.g., Eggler and Kadik, 1979; Holloway, 1977). Of particular interest to our research group has been (1) the determination of activity coefficients of H_2O ($\gamma_{\text{H}_2\text{O}}$) in $\text{H}_2\text{O--CO}_2$ vapors coexisting with aluminosilicates (Bohlen et al. 1982; Bohlen et al., 1983) and (2) the use of phase equilibria to shed light on the thermal and structural properties of aluminosilicate liquids (Boettcher et al., 1982a; 1982b).

Towards these goals, Bohlen et al. (1982) experimentally determined the *vapor-saturated solidi* in the system $\text{NaAlSi}_3\text{O}_8(\text{Ab})\text{--H}_2\text{O--CO}_2$ up to 25 kbar for various mole fractions of H_2O component in the vapor ($X_{\text{H}_2\text{O}}^{\text{V}}$) from nearly pure H_2O ($X_{\text{H}_2\text{O}}^{\text{V}} \sim 1.0$) to nearly pure CO_2 ($X_{\text{H}_2\text{O}}^{\text{V}} = 0$). These results revealed that CO_2 produces no detectable freezing-point depression and is essentially insoluble below about 15 kbar in the high-temperature, CO_2 -rich part of the system. However, the solubility of CO_2 in the lower-temperature $\text{Ab--H}_2\text{O--CO}_2$ liquids could not be determined from our results, and for purposes of calculating values of $\gamma_{\text{H}_2\text{O}}$, it was assumed to be zero. In this and all other recent studies in our laboratory, care was

exercised to remove external sources of H_2O and H_2 that would affect phase relationships (Boettcher et al., 1981).

The values of $\gamma_{\text{H}_2\text{O}}^{\text{V}}$ calculated by Bohlen et al. (1982) ranged from nearly ideal values (unity) at large values of $X_{\text{H}_2\text{O}}^{\text{V}}$ to > 5.0 at high pressures and low values of $X_{\text{H}_2\text{O}}^{\text{V}}$. Although these values are significantly lower than those calculated by Eggler and Kadik (1979) from their studies of melting, also in the system $\text{NaAlSi}_3\text{O}_8\text{--H}_2\text{O--CO}_2$, both sets of values are higher than those calculated using the Modified Redlich-Kwong formulation (e.g., Kerrick and Jacobs, 1981).

More recently, Bohlen et al. (1983) experimentally investigated melting in the system $\text{KAlSi}_3\text{O}_8(\text{Sa})\text{--SiO}_2(\text{Qz})\text{--H}_2\text{O--CO}_2$. Here, the calculated values of $\gamma_{\text{H}_2\text{O}}^{\text{V}}$, using the formulation of Burnham (1979) and the assumption that CO_2 is insoluble in the eutectic liquids, are ideal ($\gamma_{\text{H}_2\text{O}}^{\text{V}} = 1$) up to at least 15 kbar and from $X_{\text{H}_2\text{O}}^{\text{V}} = 0.1$ to 1.0, within the uncertainties of the calculated and the experimental results.

Several factors strongly suggest that the disparate results from these two systems result from greater solubility of CO_2 in the $\text{NaAlSi}_3\text{O}_8\text{--H}_2\text{O--CO}_2$ liquids than in those in the system $\text{KAlSi}_3\text{O}_8\text{--SiO}_2\text{--H}_2\text{O--CO}_2$, yielding large values for the apparent solubility of CO_2 and, therefore, large apparent values of $\gamma_{\text{H}_2\text{O}}^{\text{V}}$. First, the values of $\gamma_{\text{H}_2\text{O}}^{\text{V}}$ in the former system increase with pressure at any given value of $X_{\text{H}_2\text{O}}^{\text{V}}$, as would be expected if the solubility of CO_2 in the liquid ($X_{\text{CO}_2}^{\text{L}}$) increases with pressure. Second, the eutectic liquids in the latter system are richer in Si_4O_8 component and are more polymerized than are

¹Institute of Geophysics and Planetary Physics Contribution No. 2465.

the liquids in the former, and the solubility of CO_2 is expected to be less (e.g., Mysen et al., 1976).

As a result of these uncertainties, I investigated melting relationships in the system $\text{SiO}_2(\text{Qz})\text{-H}_2\text{O-CO}_2$, which has advantages compared to feldspar-bearing systems because of the compositional simplicity. The solubility of carbon-bearing species in silicate liquids is commonly thought to be predominantly as CO_3^{2-} anion (e.g., Mysen and Virgo, 1980), requiring (1) divalent or monovalent cations such as K^+ or Ca^{2+} for charge-balance, and (2) non-bridging oxygen (NBO) ions. The system $\text{SiO}_2\text{-CO}_2$ has neither of these characteristics, but in the system $\text{SiO}_2\text{-H}_2\text{O-CO}_2$, if water dissolves as OH by breaking bonds between tetrahedra, NBO ions and H^+ are created, and CO_3^{2-} may form in the liquid. Alternatively, CO_3^{2-} may not be stable in these liquids, and molecular CO_2 or C may be significant species.

Experimental methods

Starting materials (reactants)

Natural Brazilian quartz was ground under reagent-grade acetone to about 200 mesh, leached in hot HNO_3 , and fired at 1100°C for at least 24 hours and then at 800°C for at least 12 hours. Boiled, doubly distilled, deionized water was used as a source of H_2O . For nearly all experiments, the source of CO_2 was silver oxalate ($\text{Ag}_2\text{C}_2\text{O}_4$), which was dried under soft vacuum at 40°C for at least 48 hours and stored in a vacuum desiccator over KOH. Each batch of the $\text{Ag}_2\text{C}_2\text{O}_4$ was checked for purity and stoichiometry by the method described by Bohlen et al. (1982). For some of the experiments to prepare Ag-free glasses for spectral analyses and to compare results using different sources of CO_2 , oxalic acid (dihydrate) was used. However, uncertainties in the content of H_2O in oxalic acid precludes using it as a source of CO_2 for experiments to determine the *vapor-saturated solidi*.

For each experiment, ~4 to 30 mg of quartz and appropriate amounts (Table 1) of $\text{Ag}_2\text{C}_2\text{O}_4$ and/or H_2O were loaded into 2.0-mm diameter Pt capsules welded at each end. These sealed capsules were in turn placed into 3.5-mm diameter Pt capsules with 150–160 mg of sintered hematite (Boettcher et al., 1973), which maintains a low f_{H_2} and low f_{CO} during the experiments. Special care was required to ensure that the desired quantities of H_2O and $\text{Ag}_2\text{C}_2\text{O}_4$ remained in the capsules until after they were sealed. The H_2O was loaded and immediately covered with a thin circle of Pt foil to prevent evaporation. Numerous tests demonstrated that this method prevented measurable loss of H_2O that otherwise occurs within several minutes. The capsules were handled only with special pliers during loading; touching them with the hands warmed them and increased evaporation. All weights were measured on a Mettler M-5 microbalance, reproducible to ± 0.000002 gr.

Apparatus and run procedure

All experiments were conducted in piston-cylinder apparatus with a 25.4-mm diameter furnace assembly and piston. The assembly was constructed of NaCl, BN, AlSiMag, and glass (Boettcher et al., 1981); no hydrous phases such as talc were used, and all lubricants were fluorocarbons to eliminate most sources of H_2 . Temperatures were measured and controlled with

$\text{WRe}_3\text{-WRe}_{25}$ thermocouples. We used the piston-in technique by bringing the pressure to about 5% below the final value, and then increasing the temperature and pressure, respectively, to the desired values. The furnace assembly was calibrated as described by Bohlen et al. (1982), revealing that the furnace assembly requires no pressure correction.

The *vapor-saturated solidi* for the various $\text{H}_2\text{O}/\text{CO}_2$ compositions were determined by noting the temperature of the first appearance of quenched liquid in the run products. To check the attainment of equilibrium for the determination of the *vapor-saturated solidi*, reversal experiments were conducted in two-stage runs. Here, the initial conditions were those known from other experiments to produce partial melting. The conditions were next changed isobarically to about 10°C below the inferred *vapor-saturated solidus* and held for sufficient time to react away all liquid, as evidenced by no quenched liquid in the run products.

Run products

After the experiments, the hematite, which partially reacts to magnetite during the experiment, was examined optically to ensure that sufficient (>~20%) hematite remained unreacted. The inner capsule was cleaned and boiled in dilute HCl to remove all traces of the hematite-magnetite buffer. It was then weighed, held at -5°C for at least 15 minutes, punctured with a fine needle, reweighed, dried at 112°C for 15 minutes, and reweighed. This procedure permitted verification that the H_2O and CO_2 in the reactants remained throughout the experiment. Successful runs had $\text{H}_2\text{O}/\text{CO}_2$ ratios usually within 1 mole% of the initial value, except for experiments well above the beginning of melting in which significant amounts of fluid remain in the quenched liquid. Also, the sample capsule would be puffed and hiss audibly when punctured.

The reactants were examined optically in immersion oils. The quartz occurred mostly as anhedral fragments, but euhedra were common in some runs. Attempts to locate the $\alpha \rightleftharpoons \beta$ quartz transformation by the morphology of the quenched quartz or by visual evidence of strain in crystals passing through the transformation during quenching were unsuccessful.

The appearance of the quenched liquid varied with the conditions of the experiment. At the lower pressures, liquids quenched to bubble-rich glass, resulting from exsolution of H_2O and CO_2 during quenching. At pressures above ~15 kbar, the liquids dissolve sufficient volatile components to render them black, even opaque and reflective, during quenching (see Boettcher and Wyllie, 1969, especially Plate 1).

Quenched vapor occurs in several forms, commonly in the same experiment. The most obvious forms at pressures below ~15 kbar are the easily recognized glass spheres, appearing individually or in aggregates resembling fish roe. Also common are large (up to 0.5 mm), thin, generally bubble-free plates of glass, which are more abundant than the spheres at higher pressures. In these experiments with H_2O -rich vapors, critical points were encountered where the liquid and vapor coexisting with quartz become identical in all respects. As the critical points are approached from lower pressures, the quenched vapors become more abundant and more like the quenched liquid in appearance. At pressures above those of the critical point, there is no first-order transformation (melting), and the ratio of quenched fluid to quartz increases with increasing temperature until quartz disappears at a temperature that is a function of the bulk composition, as discussed below.

In some experiments, particularly near the *vapor-saturated liquid*, several percent or less quartz crystallized from the liquid during the quench. Commonly, when the experiment was repeated under similar or the same conditions, no crystalline phase appeared in the run products. The quench quartz was easily recognized by the sheafs of radial intergrowths, commonly in spherical aggregates.

Experimental results

Experimental data are presented in Table 1 and in Figure 1. For simplicity, these data are discussed in terms of the bounding sub-systems.

SiO_2

At its melting temperature at atmospheric pressure, β -quartz is presumably metastable with respect to tridymite (Fig. 1). However, the quartz \rightleftharpoons tridymite reaction is extremely sluggish at this temperature (if it occurs at all), and MacKenzie (1960) was able to experimentally partially fuse quartz at 1450°C in 2 hours, but no evidence of reaction occurred at 1400°C for a similar duration. Although the lower limit is uncertain, these data are consistent with the values of Gibbs free energy of fusion recently compiled by Richet et al. (1982). Following Richet et al., I have adopted a temperature of 1700 K (1427°C).

The melting of β -quartz from 7 to 25 kbar was experimentally determined by Jackson (1976). If we adopt his triple point between cristobalite, β -quartz, and liquid and the fusion temperature of cristobalite at atmospheric pressure of Greig (1927), then the fusion curve of cristobalite has a negative dP/dT slope (Fig. 1). The uncertainties in the high-temperature part of this system are large.

$\text{SiO}_2\text{-H}_2\text{O}$

Previous investigations in this system that bear on this study are those of Kennedy et al. (1962) and Stewart (1967) to pressures of 10 kbar; Ostrovskii et al. (1959) determined the temperature of the beginning of melting to vapor pressures of about 5 kbar. The results of all three studies are consonant with a temperature of $1130 \pm 10^\circ\text{C}$ for the vapor-saturated solidus at 2 kbar. At 5 kbar, the brackets of Kennedy et al., Stewart, and Ostrovskii et al. are 1089–1095°C, 1055–1070°C, and $\sim 1080^\circ\text{C}$. Similarly, at about 10 kbar, the values of Stewart (1040–1050°C) are lower than those of Kennedy et al. (1073–1086°C). The results of this study from 7 to 10 kbar are intermediate between those of Stewart and Kennedy et al. (e.g., 1060–1070°C at 9 kbar). The *vapor-saturated solidus* in Figures 1 and 2 is based on my brackets at 7 and 9 kbar and an average of the Kennedy et al. and Stewart data at 5 kbar.

Kennedy et al. concluded that the *vapor-saturated solidus* terminates at a critical end-point (point K_2^1 in Fig. 1), where the liquid and vapor in equilibrium with quartz are equal in all respects. Stewart's data suggest that K_2^1 should be somewhat above 10 kbar. Because the compositions of liquid and vapor change markedly with pressure

Table 1. Experimental results for $\text{SiO}_2\text{-H}_2\text{O-CO}_2$

Run #	$X_{\text{H}_2\text{O}}^{\text{V}}$	$\text{H}_2\text{O}+\text{CO}_2$ wt%	Pres Kbar	Temp °C	Duration Hrs	Products
713	1.0	20	7.0	1060	3.0	Qz+V
550	1.0	19.4	7.0	1065	4.0	Qz+L+V
258R	1.0	20	7.0	1070	3	(see #550)
			7.0	1055	4	Qz+(L)+V
254	1.0	20	9.0	1050	2.0	Qz+V
263	1.0	20	9.0	1060	2.0	Qz+V
257	1.0	20	9.0	1070	2.0	Qz+L+V
255	1.0	20	9.0	1080	2.0	Qz+L+V
256	1.0	20	9.0	1090	2.0	Qz+L+V
668	1.0	20	11.0	1030	2.0	Qz+F
666	1.0	20	11.0	1060	2.0	Qz+F
667	1.0	20	11.0	1090	2.0	Qz+F
548	1.0	18	17.0	1380	2.0	L
549	1.0	15	17.0	1380	2.0	(Qz+L)
761	0.95	27	9.5	1075	6.0	Qz+V
762	0.95	27	9.5	1085	6.0	Qz+L+V
763	0.95	27	9.5	1095	6.0	Qz+L+V
794	0.95	27	11.0	1065	4.0	Qz+V
768	0.95	27	11.0	1080	4.0	Qz+L+V
757	0.95	28	12.0	1055	6.0	Qz+V
754	0.95	23	12.0	1075	6.0	Qz+V
682	0.95	27	15.0	1050	8.0	Qz+V
735	0.95	27	15.0	1070	3.0	Qz+V
738	0.95	28	15.0	1080	3.0	Qz+L
721	0.95	26	15.0	1100	3.0	Qz+L
691	0.95	25	15.0	1125	4.0	Qz+L
701	0.95	26	19.5	1070	4.0	Qz+V
697	0.95	27	19.5	1090	3.0	Qz+V
696	0.94	27	19.5	1140	3.0	Qz+V
815	0.95	27	21.0	1065	4.0	Qz+V
809	0.95	27	23.0	1025	3.0	Qz+V
811	0.95	27	23.0	1040	3.0	Qz+V
799	0.95	27	23.0	1050	3.0	Qz+V
742	0.95	25	23.0	1070	3.0	Qz+V
789	0.925	25	13.5	1090	4.0	Qz+V
792	0.926	25	13.5	1100	4.0	Qz+L+V
795	0.925	25	13.5	1110	4.0	Qz+V
773	0.925	25	15.0	1085	4.0	Qz+V
775	0.925	25	15.0	1095	4.0	Qz+L+V
771	0.925	25	15.0	1115	4.0	Qz+L+V
779	0.925	25	16.0	1080	4.0	Qz+V
780	0.925	25	16.0	1100	4.0	Qz+L+V
783	0.926	25	16.0	1095	4.0	Qz+L+V
785	0.924	25	17.0	1075	4.0	Qz+V
808	0.925	25	17.0	1090	4.0	Qz+L+V
813	0.926	25	19.0	1050	4.0	Qz+V
818	0.926	25	20.0	1060	4.0	Qz+L+V
822	0.926	25	21.5	1040	3.0	Qz+V
824	0.926	25	21.5	1055	3.0	Qz+(L)+V
827	0.926	25	21.5	1065	3.0	Qz+L+V
829						
655	0.89	26	7.5	1105	4.3	Qz+V
664	0.90	27	7.5	1120	5.0	Qz+L+V
435	0.90	29	10.0	1095	4.0	Qz+V
465	0.90	27	10.0	1105	5.0	Qz+V
469	0.90	26	10.0	1115	5.0	Qz+L+V
467	0.90	28	10.0	1125	5.0	Qz+L+V
676R	0.90	27	10.0	1125	4.0	(see #467)
			10.0	1100	24.0	Qz+V
758	0.91	27	12.5	1110	4.0	Qz+V
745	0.89	28	12.5	1120	3.0	Qz+L+V
505	0.91	26	15.0	1075	7.0	Qz+V
474	0.90	25	15.0	1095	6.0	Qz+V
473	0.90	29	15.0	1115	6.0	Qz+V
475	0.90	29	15.0	1125	5.0	Qz+L
628	0.90	25	15.0	1150	5.0	Qz+L+V
726a	0.90	49	15.0	1350	4.0	L+V
810	0.90	27	16.0	1120	4.0	Qz+L+V
747	0.91	27	17.5	1105	3.0	Qz+L+V
751	0.90	26	17.5	1115	6.0	Qz+L+V
637	0.90	26	17.5	1140	5.0	Qz+L+V
787	0.90	27	18.0	1075	4.0	Qz+V
786	0.90	27	18.0	1085	4.0	Qz+V
794	0.95	27	11.0	1065	4.0	Qz+V
633	0.90	25	20.0	1135	4.5	Qz+L+V
743	0.90	26	20.5	1105	3.0	Qz+L+V
736	0.89	26	20.5	1125	3.0	Qz+L+V
731	0.90	27	20.5	1125	3.0	Qz+L+V
800	0.90	27	21.5	1095	4.0	Qz+L+V
718	0.90	26	22.5	1100	3.0	Qz+L+V
715	0.91	25	22.5	1120	3.0	Qz+L+V
797	0.90	27	23.0	1080	4.0	Qz+V
806	0.90	27	25.0	1075	4.0	Qz+V
709	0.89	27	25.0	1085	4.0	Qz+L+V
642	0.90	27	25.0	1110	5.0	Qz+L+V
643	0.89	26	25.0	1130	4.0	Qz+L+V
646	0.91	26	25.0	1165	3.0	Qz+L+V
647	0.79	27	7.5	1125	10.0	Qz+V
611	0.79	26	7.5	1150	10.0	Qz+L+V

Table 1. (cont.)

Run #	X _{H₂O} ^v	H ₂ O+CO ₂ wt. %	Pres Kbar	Temp °C	Duration Hrs	Products
616	0.80	27	7.5	1170	10.0	Qz+L+V
627	0.80	26	7.5	1185	10.0	Qz+L+V
371	0.80	27	10.0	1120	10.0	Qz+V
370	0.80	22	10.0	1130	10.0	Qz+V
372	0.80	23	10.0	1140	10.0	Qz+L+V
366	0.80	23	10.0	1150	10.0	Qz+L+V
674R	0.80	27	10.0	1150	4.0	(see #366)
			10.0	1120	24.0	Qz+V
			12.5	1140	8.0	Qz+V
619	0.79	27	12.5	1140	8.0	Qz+V
638	0.79	26	12.5	1150	8.0	Qz+L+V
376	0.80	26	15.0	1120	10.0	Qz+V
383	0.80	25	15.0	1140	10.0	Qz+V
386	0.80	26	15.0	1150	10.0	Qz+(L)+V
384	0.80	25	15.0	1160	10.0	Qz+L+V
485R	0.80	29	15.0	1160	8.0	(see #384)
			15.0	1135	14.5	Qz+V
			15.0	1260	6.0	Qz+L+V
428	0.80	27	15.0	1260	6.0	Qz+L+V
458	0.80	49	15.0	1280	5.0	(Qz)+L+V
454	0.80	49	15.0	1290	5.0	L+V
453	0.80	47	15.0	1310	6.0	L+V
446	0.80	49	15.0	1350	6.0	L+V
695oa	0.78	31	15.0	1350	4.0	(Qz)+L+V
801	0.80	30	15.0	1360	4.0	L+V
392	0.80	25	18.0	1135	6.0	Qz+V
385	0.80	22	18.0	1150	10.0	Qz+L+V
422	0.80	28	20.0	1125	10.0	Qz+V
427	0.77	29	20.0	1132	10.0	Qz+V
415	0.81	24	20.0	1140	10.0	Qz+L+V
397	0.80	27	20.0	1145	10.0	Qz+L+V
702oa	0.79	51	22.0	1275	4.0	L+V
755	0.78	26	22.5	1110	4.0	Qz+V
760	0.80	31	22.5	1110	4.0	Qz+V
744	0.79	26	22.5	1125	8.0	Qz+L+V
455	0.80	26	25.0	1100	6.0	Qz+V
456	0.80	29	25.0	1110	5.0	Qz+V
439	0.80	50	25.0	1125	10.0	Qz+L+V
770oa	0.80	50	25.0	1275	4.0	L+V
790oa	0.80	50	25.0	1300	5.0	L+V
784	0.80	50	25.0	1300	5.0	20%q+L
750	0.80	41	27.5	1085	8.0	Qz+V
710	0.80	27	27.5	1105	2.0	Qz+V
714	0.80	27	27.5	1105	2.0	Qz+V
730	0.80	27	27.5	1115	2.0	Qz+L+V
748	0.79	40	27.5	1130	4.8	Qz+V
733	0.79	27	27.5	1130	2.0	Qz+V
752	0.80	35	27.5	1145	4.0	Qz+L+V
807	0.70	27	7.5	1195	7.0	Qz+V
600	0.70	27	7.5	1200	7.0	Qz+V
601	0.69	26	7.5	1210	7.0	Qz+V
788	0.70	27	7.5	1210	7.0	Qz+L+V
609	0.70	27	7.5	1220	6.0	Qz+L+V
368	0.69	30	10.0	1180	8.0	Qz+V
367	0.70	28	10.0	1190	8.0	Qz+V
369	0.71	29	10.0	1200	8.0	Qz+L+V
365	0.69	30	10.0	1210	8.0	Qz+L+V
675R	0.70	27	10.0	1220	4.0	(see #365)
			10.0	1180	24.0	Qz+V
			12.5	1170	7.0	Qz+V
618	0.70	27	12.5	1180	9.0	Qz+V
614	0.69	25	12.5	1180	9.0	Qz+L+V
587	0.70	27	12.5	1190	8.0	Qz+L+V
421	0.69	28	12.5	1200	8.0	Qz+L+V
425	0.69	28	15.0	1185	10.0	Qz+V
373	0.70	28	15.0	1195	8.0	Qz+(L)+V
374	0.69	27	15.0	1205	8.0	Qz+L+V
653oa	0.70	42	15.0	1370	5.0	L+V
388	0.70	28	20.0	1180	10.0	Qz+V
381	0.69	30	20.0	1190	8.0	Qz+L+V
377	0.70	30	20.0	1210	8.0	Qz+L+V
654oa	0.70	43	20.0	1400	4.0	L+V
686	0.70	42	20.0	1400	4.0	L+V
396	0.69	28	25.0	1160	10.0	Qz+V
414	0.70	26	25.0	1175	8.0	Qz+V
391	0.70	26	25.0	1190	8.0	Qz+L+V
420	0.68	28	25.0	1200	8.0	Qz+L+V
764	0.70	26	27.5	1160	3.0	Qz+V
759	0.69	26	27.5	1175	3.0	Qz+L+V
605	0.60	27	7.5	1210	6.0	Qz+V
599	0.60	27	7.5	1220	6.0	Qz+V
613	0.60	27	7.5	1230	6.0	Qz+L+V
457	0.61	27	10.0	1210	6.0	Qz+V
451	0.61	27	10.0	1220	5.0	Qz+V
449	0.59	28	10.0	1230	5.0	Qz+L+V
448	0.61	27	10.0	1240	5.0	Qz+L+V
447	0.61	25	10.0	1255	5.0	Qz+L+V
438	0.58	27	12.5	1245	8.0	Qz+V
436	0.61	26	12.5	1260	8.0	Qz+L+V
719oa	0.60	50	16.0	1435	3.0	L+V
492	0.62	29	16.5	1245	6.0	Qz+V
491	0.61	31	16.5	1255	6.0	Qz+L+V
470	0.60	28	16.5	1275	5.0	Qz+L+V
659r	0.60	26	16.5	1265	5.0	(see #470)
			16.5	1240	5.0	Qz+L+V

Table 1. (cont.)

Run #	X _{H₂O} ^v	H ₂ O+CO ₂ wt. %	Pres Kbar	Temp °C	Duration Hrs	Products
497R	0.60	28.6	16.5	1265	2.0	(see #470)
			16.5	1240	24.0	Qz+V
			20.0	1255	24.0	Qz+V
481	0.58	26	20.0	1255	5.0	Qz+V
442	0.59	27	20.0	1260	5.0	Qz+V
482	0.63	28	20.0	1265	24.0	Qz+L+V
443	0.58	29	20.0	1270	5.0	Qz+V
441	0.60	28	20.0	1280	4.0	Qz+L+V
440	0.61	27	20.0	1300	4.0	Qz+L+V
477r	0.60	29	20.0	1285	4.0	(see #441)
			20.0	1260	8.0	Qz+L+V
			20.0	1285	4.0	(see #441)
478r	0.60	25	20.0	1260	16.0	Qz+L+V
			20.0	1285	4.0	(see #441)
486R	0.60	29	20.0	1285	4.0	(see #441)
			20.0	1255	17.3	Qz+V
			22.5	1255	3.0	Qz+V
590	0.60	26	22.5	1255	3.0	Qz+V
585	0.60	27	22.5	1255	4.0	Qz+V
495	0.59	29	22.5	1255	6.0	Qz+V
472	0.60	28	22.5	1265	5.0	Qz+L+V
487	0.60	27	24.0	1240	8.0	Qz+V
488	0.59	29	24.0	1240	8.0	Qz+V
732oa	0.60	51	24.0	1430	2.0	Qz+L+V
737oa	0.59	51	24.0	1470	1.5	L+V
466	0.60	28	25.0	1230	6.0	Qz+V
468	0.60	32	25.0	1240	6.0	Qz+(L)+V
464	0.60	28	25.0	1250	5.0	Qz+L+V
460	0.59	28	25.0	1260	5.0	Qz+L+V
459	0.61	28	25.0	1285	5.0	Qz+L+V
644	0.51	27	7.5	1280	2.0	Qz+V
639	0.50	26	7.5	1300	2.0	Qz+L+V
636	0.50	27	7.5	1312	2.0	Qz+L+V
629	0.50	26	7.5	1325	2.0	Qz+L+V
356	0.50	30	10.0	1280	2.0	Qz+V
363	0.50	32	10.0	1290	2.0	Qz+V
382	0.50	26	10.0	1310	2.0	Qz+V
390	0.49	33	10.0	1318	2.0	Qz+L+V
364	0.51	32	10.0	1325	2.0	Qz+L+V
493	0.48	28	12.5	1320	2.0	Qz+V
499	0.50	29	12.5	1330	2.0	Qz+L+V
399	0.50	30	15.0	1325	6.0	Qz+V
401	0.49	31	15.0	1345	4.0	Qz+L+V
665oa	0.50	30	15.0	1350	4.0	Qz+L+V
305	0.50	31	16.0	1330	1.0	Qz+V
294	0.50	23	16.0	1320	2.0	Qz+V
298	0.50	28	16.0	1350	1.0	Qz+L+V
483	0.49	26	17.5	1350	4.0	Qz+V
479	0.50	30	17.5	1370	3.0	Qz+L+V
288	0.50	29	18.0	1340	1.0	Qz+L+V
309	0.50	32	20.0	1340	2.0	Qz+V
314	0.49	29	20.0	1350	2.0	Qz+V
335	0.49	35	20.0	1370	1.0	Qz+L+V
408	0.50	28	20.0	1390	1.0	Qz+L+V
409	0.48	23	20.0	1400	1.0	Qz+(L)+V
489	0.50	29	21.0	1375	2.0	Qz+L+V
490	0.48	29	21.0	1375	2.0	Qz+(L)+V
484	0.51	30	21.0	1410	2.0	Qz+L+V
500	0.51	28	22.5	1375	2.0	Qz+L+V
598	0.50	27	23.0	1364	2.0	Qz+L+V
324	0.50	31	24.0	1370	1.0	Qz+L+V
597	0.50	27	25.0	1350	2.0	Qz+V
586	0.50	27	25.0	1365	2.0	Qz+L+V
337	0.50	31	26.0	1320	0.5	Qz+V
502	0.30	28	12.5	1475	0.5	Qz+V
503	0.28	27	12.5	1500	0.5	Qz+L+V
510	0.30	27	12.5	1520	0.5	Qz+L+V
512	0.30	27	12.5	1520	0.3	Qz+L+V
398	0.30	24	15.0	1470	0.5	Qz+V
405	0.30	24	15.0	1510	0.5	Qz+V
430	0.30	37	15.0	1530	0.3	Qz+L+V
423	0.30	27	15.0	1560	0.3	Qz+L+V
645	0.30	26	17.5	1575	0.1	Qz+L+V
620	0.30	27	20.0	1590	0.2	Qz+V
631	0.30	27	20.0	1610	0.1	Qz+V
608	0.30	27	20.0	1622	0.1	Qz+L+V

Abbreviations: Qz=quartz, L=liquid, V=vapor, F=supercritical fluid, q=quartz formed on quench (not indicated for all runs where it occurs), R=successful reversal, r=attempted reversal, oa=oxalic acid used as source of CO₂; all other runs used Ag₂C₂O₄, ()=trace amount.

near the critical end-point (e.g., see Kennedy et al., Fig. 8), the exact pressure is difficult to establish. A pressure of 10 kbar is consistent with my results at 9 kbar, where the beginning of melting was bracketed between 1060 and 1070°C, and at 11 kbar, where no first-order melting

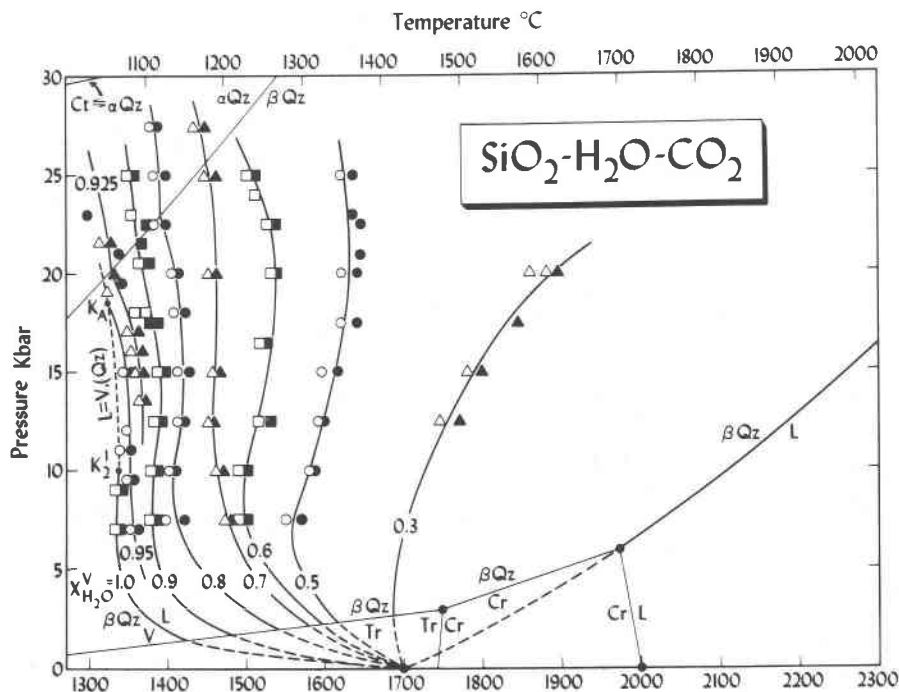


Fig. 1. Pressure-temperature projection of the *vapor-saturated solidi* of quartz + vapor for various values of the mole fraction of H_2O in the $\text{H}_2\text{O-CO}_2$ vapor ($X_{\text{H}_2\text{O}}^{\text{V}}$). Closed symbols represent quartz + liquid + vapor; open symbols are quartz + vapor. Parts of some of the curves purposefully do not pass between the brackets (see text). The fusion of quartz + H_2O below 7 kbar is from Stewart (1967) and Kennedy et al. (1962). The metastable fusion of quartz at atmospheric pressures is from Richet et al. (1982) and agrees with the experimental value of <1723 K of MacKenzie (1960); the fusion of quartz at high pressure is from Jackson (1976). Cohen and Klement (1967) determined the α - β quartz transition, and Bohlen and Boettcher (1982) determined the coesite-quartz transition. The negative slope of the fusion curve of cristobalite results from fitting Jackson's data to the accepted fusion temperature of cristobalite at atmospheric pressure (Greig, 1927). The dashed curves for quartz-bearing assemblages are metastable with respect to tridymite- or cristobalite-bearing ones. The dashed curve connecting the points K_2^1 and K_A^1 is the ternary locus of points where critical fluid coexists with quartz [$\text{L} = \text{V}, (\text{Qz})$].

reaction was observed and all of the run products contained glass that resembles quench liquid. A pressure of 10 kbar for K_2^1 is also consistent with the critical phenomena in the ternary system, as discussed below.

$\text{SiO}_2\text{-H}_2\text{O-CO}_2$

There are no previous studies of melting relationships in this system. However, Shettel (1973) investigated the solubility of quartz in the vapor in this system at 500–900°C at 5 kbar, and Nakamura (1974) studied the effects of reduced activities of H_2O on melting in the system $\text{SiO}_2\text{-H}_2\text{O}$.

The results of the experiments for various values of mole fraction of H_2O in the vapor ($X_{\text{H}_2\text{O}}^{\text{V}}$) are shown in Table 1 and Figure 1. In this figure, it should be noted that the *vapor-saturated solidi* do not always pass between the illustrated experimental brackets. This occurs because some of the capsules contain a slight excess or deficiency of H_2O relative to CO_2 (see Table 1), and the beginning of melting is thus slightly shifted up or down in temperature relative to the values expected for the labeled curves.

Some comparison experiments (e.g. #2665 for $X_{\text{H}_2\text{O}}^{\text{V}} =$

0.5) in Table 1 were performed with oxalic acid ($\text{C}_2\text{H}_2\text{O}_4 \cdot 2\text{H}_2\text{O}$) as a source of CO_2 to ensure that the Ag in the $\text{Ag}_2\text{C}_2\text{O}_4$ did not affect phase relationships. However, a rigorous comparison is not possible because of the uncertainties in the H_2O content of oxalic acid (Boettcher et al., 1973). Experiments with $\text{Ag}_2\text{C}_2\text{O}_4$ and $\text{C}_2\text{H}_2\text{O}_4 \cdot 2\text{H}_2\text{O}$ were performed at the various *vapor-saturated liquids* to elucidate phase relationships, which are discussed below, and to prepare glasses for Raman and infrared spectroscopy.

The *vapor-saturated solidi* for the larger values of ($X_{\text{H}_2\text{O}}^{\text{V}}$) intersect the $\alpha\text{Qz} \rightleftharpoons \beta\text{Qz}$ transition boundary as determined by Cohen and Klement (1967). This transition may not be first-order, i.e., it may not exhibit a discontinuity in entropy or volume (Klement and Cohen, 1968, p. 2257), but such discontinuities ($\Delta_m S$ and $\Delta_m V$) are consistent with the brackets in Figure 1 and with changes in the slopes of univariant curves in other systems at high pressures and temperatures (e.g., Bohlen et al., 1980a; 1980b).

As shown in Figure 1, the *vapor-saturated solidi* for the H_2O -rich compositions terminate at critical points similar

to that encountered for $\text{SiO}_2\text{-H}_2\text{O}$ (K_2^1). These points (e.g., K_A for $X_{\text{H}_2\text{O}}^v = 0.95$) are unlike K_2^1 in that they are not critical end-points and they are ternary. Ternary critical end-points occur where the critical phase coexists with *two* other phases (Boettcher and Wyllie, 1969); at points such as K_A , the critical fluid ($L = V$) coexists with quartz only.

The curves in Figure 1 labelled 0.95, 0.8, 0.6, etc., including that terminated by point K_A , are isopleths (constant $X_{\text{H}_2\text{O}}^v$) on a ternary, divariant surface in pressure-temperature- $X_{\text{H}_2\text{O}}^v$ space, similar to Wyllie's (1962) petrogenetic model, where solid, liquid, and vapor coexist. Although these curves are ternary and univariant, they are the loci of points where only *three* phases coexist. That is, the variance (variations of phase) of the three-phase assemblage is reduced by one because of the restriction that the ratio of $\text{H}_2\text{O}/\text{CO}_2$ is constant along each curve.

The H_2O -rich part of the ternary, three-phase surface terminates along a smooth curve connecting points K_2^1 , K_A , etc.; the termination is shown in projection in Figure 1 as the dashed curve $L = V$, (Qz), using the notation of Greig (1954). For compositions with $X_{\text{H}_2\text{O}}^v$ equal to or less than about 0.9, vapors and liquids remain as discreet phases to the highest pressures investigated (27.5 kbar). Although the solubility of carbon in the hydrous SiO_2 liquids increases markedly above about 10–15 kbar, the solubility of SiO_2 component in the vapors remains too low to form a critical point; that is, the miscibility gap between the liquids and vapors does not close. This is consonant with the conclusions of Shettel (1973) at 5 kbar that CO_2 greatly diminishes the solubility of SiO_2 in the vapor. The trajectory of the $L = V$, (Qz) curve is drawn to be consistent with the conclusion of Kennedy et al. (1962) that the critical end-point for $\text{SiO}_2\text{-H}_2\text{O}$ is near 10 kbar.

Properties of liquids and vapors

Two of the major reasons for investigating this system were (1) to establish the conditions, if any, at which activity coefficients for H_2O in the vapor ($\gamma_{\text{H}_2\text{O}}^v$) could be determined from the phase relationships and (2) to determine the solubility, if detectable, of carbon in the ternary liquids and to use these data to shed light on the structures of the liquids.

Activity of H_2O in the $\text{H}_2\text{O-CO}_2$ vapor

Our earlier results in the system $\text{NaAlSi}_3\text{O}_8\text{-H}_2\text{O-CO}_2$ did not allow calculation of $\gamma_{\text{H}_2\text{O}}^v$ because of the significant, but unknown, quantities of carbon dissolved in the liquids; that is, the freezing-point depression attributable to H_2O was unknown. Although our results in the system $\text{KAlSi}_3\text{O}_8\text{-SiO}_2\text{-H}_2\text{O-CO}_2$ are consistent with values of $\gamma_{\text{H}_2\text{O}}^v$ equal to unity, we had to assume that carbon was totally insoluble in the liquid below 15 kbar; although not unreasonable for such SiO_2 -rich compositions, this assumption remains unsubstantiated.

Similarly, to compare the experimental results (Fig. 1) in the $\text{SiO}_2\text{-H}_2\text{O-CO}_2$ system with those calculated assuming $\gamma_{\text{H}_2\text{O}}^v = \text{unity}$, I used the procedure of Burnham (1981; 1979, particularly p. 446–448 and 458–461) to calculate the relationships in Figure 2. I calculated a value of 0.233 cal/bar for Si_4O_8 for the volume of melting of quartz ($\Delta_m V_{Qz}$) using the fusion curve of Jackson (1976) and the Gibbs free energy of melting ($\Delta_m G_{Qz}^\circ$) of Richet et al. (1982); this value compares favorably with the value of 0.232 cal/bar proposed by Burnham (1981). The values of $\Delta_m G_{Qz}^\circ$ of Richet et al. at lower temperatures do not agree with those derived from the experimental $\text{SiO}_2\text{-H}_2\text{O}$ liquidus. Therefore, I calculated $\Delta_m G_{Qz}^\circ$ values using the solubility data of Kennedy et al. ($X_{\text{H}_2\text{O}}^l = 0.398$ for Si_4O_8 at 2.0 kbar, 1125°C) and equations 16-12 and 16-14 of Burnham (1979). This calculated value of $\Delta_m G_{Qz}^\circ$ at 1398 K is 2313 cal, compared to 1386 cal from Richet et al. and 2267 cal from Burnham (1981, p. 207, assuming a melting temperature of quartz of 1715 K).

Clearly, there are many uncertainties involved in the calculated curves in Figure 2, as evidenced by the discrepancies in the positions of the curves of $X_{\text{H}_2\text{O}}^v = 1.0$ and 0.0 compared to those determined experimentally. Nevertheless, the calculated curves do serve as a basis for discussion of the experimental results. In the calculated version, the temperatures of the curves for the various values of $X_{\text{H}_2\text{O}}^v$ increase at a nearly constant rate at any given pressure; similar configurations occur for the experimental solidi in $\text{NaAlSi}_3\text{O}_8\text{-H}_2\text{O-CO}_2$ and $\text{KAlSi}_3\text{O}_8\text{-SiO}_2\text{-H}_2\text{O-CO}_2$. However, the solidi for $\text{SiO}_2\text{-H}_2\text{O-CO}_2$ (Fig. 1) increase in temperature in an irregular, unpredictable manner. This probably results from complications in the solution of H_2O and CO_2 in the liquid, because the vapor is essentially pure $\text{H}_2\text{O-CO}_2$ at, say, 7 kbar, similar to those for the other two systems (see Egglar and Kadik, 1979, Fig. 2). I have no detailed explanation as to why this irregularity occurs in $\text{SiO}_2\text{-H}_2\text{O-CO}_2$, but not in $\text{KAlSi}_3\text{O}_8\text{-SiO}_2\text{-H}_2\text{O-CO}_2$; substitution of H^+ for K^+ (see Burnham, 1979) in the liquids of the latter system is one obvious difference in the solubility mechanisms.

Because of the complications associated with the solution of carbon in these silicate liquids, there is no way to use the melting curves to calculate $\gamma_{\text{H}_2\text{O}}^v$. At present, the best technique may be to obtain tightly constrained reversals on sub-solidus decarbonation or dehydration reactions in the presence of $\text{H}_2\text{O-CO}_2$ vapors. Until then, the near-ideal values obtainable from the $\text{KAlSi}_3\text{O}_8\text{-SiO}_2\text{-H}_2\text{O-CO}_2$ system appear to be the most reliable, and they agree fairly well with the values of $\gamma_{\text{H}_2\text{O}}^v$ of <1.5 at 700–800°C up to 15 kbar calculated from the modified Redlich-Kwong formulation (Kerrick and Jacobs, 1981).

Liquid structure and solubility mechanism of carbon

In the pressure interval up to about 10 kbar, there is no unequivocal evidence that CO_2 , or carbon in any form, is appreciably soluble in the hydrous, silicate liquids. There

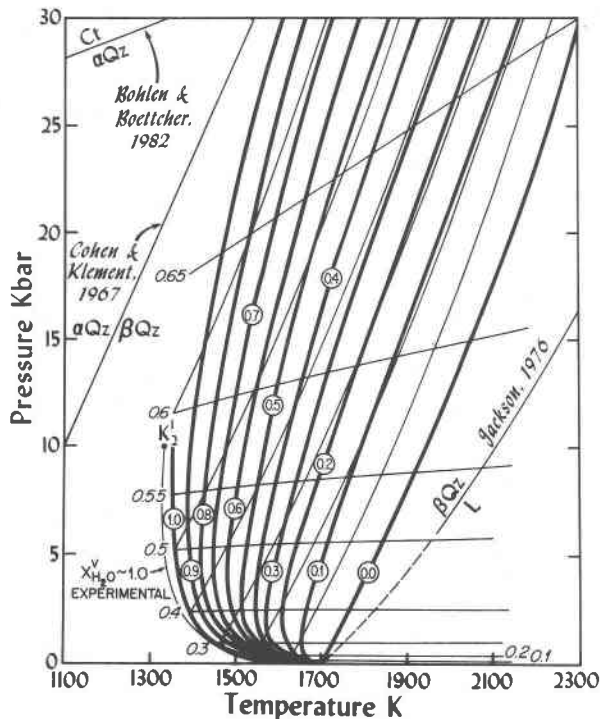


Fig. 2. Pressure-temperature projection for $\text{Si}_4\text{O}_8\text{-H}_2\text{O-CO}_2$ calculated using the method of Burnham (1979). The heavy curves are vapor-saturated solidi for the indicated values of $X_{\text{H}_2\text{O}}^{\text{V}}$. The lighter curves that are subparallel to the temperature axis are calculated isopleths (in mole%) of the solubility of H_2O in the liquid [on the L(V) surface]. The lighter curves with the steeper P - T slopes are calculated H_2O isopleths (in mole%) on the albite- H_2O liquidus [the L(S) surface]. The vapor-saturated solidus for $X_{\text{H}_2\text{O}}^{\text{V}} = 1.0$ is at the intersection of these L(S) and L(V) surfaces. K_2^1 is a critical end-point plotted at pressures determined experimentally (see Fig. 1). The experimental curve for the solidus for $X_{\text{H}_2\text{O}}^{\text{V}} \sim 1.0$ is from this study, Stewart (1967), and Kennedy et al. (1962).

is no observational evidence in the run products that suggests that carbon or CO_2 occurred in the liquids during the experiments. Also, the general configurations of the solidi in Figure 1 in this range resemble those in Figure 2, calculated assuming no solubility of carbon; however, the assumptions required to calculate these curves, including those of the activity-composition relationships in the system $\text{SiO}_2\text{-H}_2\text{O}$, possibly do not warrant this comparison.

At higher pressures, there are several lines of evidence that carbon in some form is dissolving in the liquids. First, the quenched liquids commonly contain two-phase fluid inclusions, presumably liquid H_2O and gaseous CO_2 , that exsolved during the quench. Second, curves for the beginning of melting for H_2O -rich compositions terminate at critical points, where the liquid and vapor are identical in composition. At these conditions, the ratios of the components $\text{H}_2\text{O}/\text{CO}_2$ in the liquid and vapor are the same as that in the bulk composition (assuming that no

H_2O and CO_2 dissolve in the quartz), but the absolute H_2O and CO_2 contents are unknown because the SiO_2 contents are unknown. In the system $\text{SiO}_2\text{-H}_2\text{O}$, Kennedy et al. (1962) reported that the critical fluid at the end-point contains ~ 75 wt.% (47.3 mole%) SiO_2 . A similar percentage for the ternary liquids would yield a solubility of 1.3 wt.% CO_2 at point K_A .

A third line of evidence that carbon is dissolving in the liquids at the higher pressures are the negative slopes of the melting curves in Figure 1 for $X_{\text{H}_2\text{O}}^{\text{V}} \geq 0.5$. Thus, the experimentally determined melting curves are consistent with the concept that H_2O dissolves in the SiO_2 -rich liquid (either as OH^- (Burnham, 1979) or as $\text{H}_2\text{O} + \text{OH}^-$ (Stolper, 1982)) and attains near-maximum solubility at about 15 kbar. At high pressures, carbon becomes quite soluble, resulting in the observed freezing-point depression, similar to that observed above ~ 15 kbar for $\text{NaAl-Si}_3\text{O}_8\text{-CO}_2$ (Bohlen et al., 1982). The melting curve for $X_{\text{H}_2\text{O}}^{\text{V}} = 0.3$ (Fig. 1) is remarkably similar to the calculated curve (Fig. 2); this may be the result of nearly ideal behavior and the insolubility of carbon in these higher temperature liquids.

Any proposed mechanism by which carbon dissolves in the liquids is necessarily conjectural, but some limitations are possible. Non-bridging oxygen ions and mono- or divalent cations are probably necessary for the formation of CO_3^{2-} species (Mysen and Virgo, 1980). In this system, water must dissolve as OH^- by breaking bonds between Si-O tetrahedra to produce NBO ions and H^+ . $\text{Al}_2(\text{CO}_3)_3$ is unknown as a crystalline solid and may not occur in liquids; it is less likely that $\text{Si}_2(\text{CO}_3)_4$ is a significant species in the liquid. It is conceivable that a carbon ion could be singly bonded to two bridging oxygen ions, each in different SiO_4^{4-} tetrahedra, and doubly bonded to a third bridging oxygen, but this would result in depolymerization of the liquid, rather than the polymerization observed with CO_2 in other systems (e.g., Mysen and Virgo, 1980).

It is also conceivable that carbon substitutes for Si in the tetrahedral sites of the liquid structure. Using a tetrahedral C-O bond length of 0.1378 nm estimated from the valence and electron configuration determined from the empirical trends of Brown and Shannon (1973), the closest O-O distance is ~ 0.225 nm (Wayne Dollase, UCLA, pers. comm., 1983). Although this is short relative to the 0.265 nm distances in silicates and even the 0.24 nm O-O distances in sulphates, it is comparable to the O-O distance in the planar NO_3 groups of nitrates (0.215 nm). Thus, tetrahedral carbon may be a significant component at high pressures. At present, we have insufficient data to compare the ΔV of solution as molecular CO_2 vs. that as tetrahedral carbon.

Also conceivable is the entry of carbon into the liquid as molecular CO_2 . Increased solubility of the large CO_2 molecule at high pressures in aluminosilicate liquids might result from depolymerization of the liquid as Al transforms to octahedral coordination. Similarly, the in-

crease in the solubility of CO_2 with the addition of H_2O might also result from the disruption of the liquid as H_2O breaks some of the Si-O bonds (Burnham, 1979). The first mechanism is not applicable to the system $\text{SiO}_2\text{-H}_2\text{O-CO}_2$; the latter mechanism will result in depression of the freezing point by CO_2 only if entry of the CO_2 changes the energy of the system by breaking or distorting bonds in the liquid. Simple entry of CO_2 molecules as a micro-emulsion will not produce the observed freezing-point depression. Additional evidence for the solubility of CO_2 at high pressures in this system is found in the recent work of Fine and Stolper (1983). Using infrared spectroscopy on one of the glasses synthesized in this study (run # 790), they detected only CO_2 without CO_3^{2-} .

Another possible explanation for the negative slopes of the melting curves at high pressures, and one that bears on the solubility of CO_2 , is that the liquids in the 20-kbar range undergo transitions analogous to quartz \rightleftharpoons coesite, resulting in an increase in density of the liquids. Transformations in liquids at pressures lower than those at which similar changes occur in the crystalline solids have been proposed for other systems, e.g., albite \rightleftharpoons jadeite + quartz, where Al changes from 4-fold to 6-fold coordination (Burnham, 1981; Boettcher et al., 1982a), and the electronic promotion in Cs (Klement and Jayaraman, 1966). It is conceivable that diminution of volume associated with structural changes in the liquids in the system $\text{SiO}_2\text{-H}_2\text{O-CO}_2$ contribute to the negative slopes of the fusion curves.

In a manner similar to depolymerization accompanying the change from tetrahedral to octahedral Al, the change from quartz to coesite structure in the liquid might open the structure and increase the solubility of CO_2 , although no change in the coordination of Si occurs. The configuration of the SiO_4 tetrahedra in coesite is nearly unique in that one corner of every other tetrahedron is oriented 180° to another. Thus, although the coesite structure is denser than that of quartz, the peculiar orientation of some of the tetrahedra may permit ingress of CO_2 molecules.

In summary, molecular CO_2 and/or tetrahedral carbon may be significant components in this system at high pressures, and they may also be of importance in geologically relevant aluminosilicate liquids.

Petrologic phase relationships

Phase relationships in the system $\text{SiO}_2\text{-H}_2\text{O-CO}_2$ are conceptually simple and provide a useful basis for discussion of petrologic principles in multicomponent systems with two or more volatile components. For this purpose, let us use isobaric, polythermal diagrams similar to those developed by Wyllie and Tuttle (1960) and used extensively in the literature to portray phase elements on *liquid* and *vapor-saturated liquid*. Figure 3 schematically shows three-phase triangles that illustrate the composition of coexisting solid, liquid, and vapor at isobaric, isothermal conditions. At low pressures, the solubilities of H_2O and CO_2 in the liquid [as portrayed by the curve

$L(\text{Qz},\text{V})$] are low; similarly, the solubility of SiO_2 in the vapor [$V(\text{Qz},\text{L})$] is low. At any temperature at this pressure, the compositions of the coexisting phases can be represented by a 3-phase triangle. At a pressure of ~ 10 kbar, not shown in Figure 3, the $V(\text{Qz},\text{L})$ and $L(\text{Qz},\text{V})$ curves meet at the binary critical end-point K_2^1 on the $\text{SiO}_2\text{-H}_2\text{O}$ sideline. At higher pressures, this point moves into the triangle as a ternary critical point $L = V, (\text{Qz})$, as discussed earlier. As shown in Figure 3, as the temperature in the high-pressure diagram is lowered to that of the critical point (K_A), which requires an increase in the $\text{H}_2\text{O}/\text{CO}_2$ ratio to remain in the 3-phase triangle, the compositions of the liquid and vapor coexisting with quartz approach each other, and at K_A the triangle degenerates into the tie-line $\text{SiO}_2\text{-}K_A$, connecting the composition of quartz and the coexisting critical fluid. All compositions on the line labelled 0.95 have the same $\text{H}_2\text{O}/\text{CO}_2$ ratio and have the same phases, although in different proportions, at any temperature at this or higher pressures (compositions very near the $\text{H}_2\text{O-CO}_2$ sideline are an exception, because all of the quartz dissolves in the vapor).

Consider now the beginning of melting of compositions X, X', X'', and X''' under the conditions shown in the inset of Figure 3. All of these compositions have the same $\text{H}_2\text{O}/\text{CO}_2$ ratio (i.e., the same $X_{\text{H}_2\text{O}}^Y$), and they differ only in the ratio of quartz/ $(\text{H}_2\text{O} + \text{CO}_2)$; under the conditions shown in the inset, all are in the quartz-vapor field. As the temperature is increased, and the triangle moves up-temperature, the Qz-V leg will contact all four compositions at the same temperature, and they will all then consist of quartz + liquid + vapor. Thus, the temperature

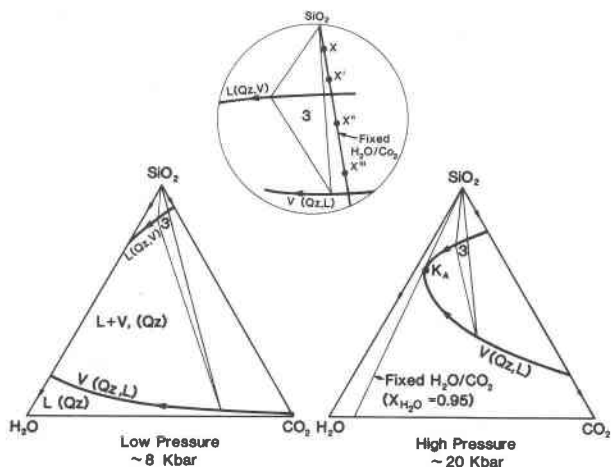


Fig. 3. Schematic isobaric, polythermal projections at low pressure (below K_2^1 , the critical end-point in the system $\text{SiO}_2\text{-H}_2\text{O}$) and at high pressure (equivalent to that of the critical point K_A in Fig. 1). Arrows on the *vapor-saturated liquidus* [$L(\text{Qz},\text{V})$] and on the *liquid-saturated vaporus* [$V(\text{Qz},\text{L})$] point down temperature. The isobaric, isothermal, 3-phase triangles show the compositions of coexisting quartz, liquid, and vapor. The inset shows the magnified area near the 3-phase triangle (see text).

of the beginning of melting [where $\text{Qz}(\text{L}, \text{V})$] is independent of the proportion of total volatiles, being dependent only on $X_{\text{H}_2\text{O}}^{\text{V}}$.

As temperature continues to rise, the divariant (isobarically univariant), 3-phase field passes over all four compositions; at sufficiently high temperatures, each of the compositions emerges from the 3-phase triangle. For the illustrated conditions, X and X' leave the triangle and enter the Qz + L field (vapor absent) at the same temperature; this is rigorously correct only if the quartz dissolves no CO_2 or H_2O components. If it does, then the Qz-V leg of the triangle will not pivot about the point SiO_2 . The *liquidus*, where $\text{L}(\text{Qz})$, for each composition is at a different temperature, as discussed below. In contrast, compositions X'' and X''' leave the 3-phase triangle and enter the L + V region, each at a different temperature [that of the *vapor-saturated liquidus*, $\text{L}(\text{Qz}, \text{V})$].

Thus, the temperature of the *vapor-saturated solidus* (beginning of melting) is dependent only on $X_{\text{H}_2\text{O}}^{\text{V}}$. For any value of $X_{\text{H}_2\text{O}}^{\text{V}}$ at a given pressure and temperature, the chemical potential of H_2O ($\mu_{\text{H}_2\text{O}}$), and those of all of the other components, are buffered. Alternatively, the temperatures of the *liquidus* and of the *vapor-saturated liquidus* are functions of $X_{\text{H}_2\text{O}}^{\text{V}}$ (i.e., $\mu_{\text{H}_2\text{O}}$ and μ_{CO_2}) and the proportion of total volatile components (i.e., the bulk composition). Therefore, when stating temperatures for the *liquidus*, *vapor-saturated liquidus*, or the upper temperature limit of a phase, it is necessary to specify the bulk composition. For example, for $X_{\text{H}_2\text{O}}^{\text{V}} = 0.8$, quartz disappears at $\sim 1280^\circ\text{C}$ for 49% $\text{H}_2\text{O} + \text{CO}_2$ and at $\sim 1350^\circ\text{C}$ for 31% $\text{H}_2\text{O} + \text{CO}_2$ at 15 kbar (Table 1).

It is not difficult to demonstrate that these principles apply to systems with more components and to systems that exhibit crystalline solution involving the non-volatile components. If the mineral phases in this or in more complex systems contain CO_2 and/or H_2O component, then every composition for a given $X_{\text{H}_2\text{O}}^{\text{V}}$ will have a unique $\mu_{\text{H}_2\text{O}}$ and temperature for the beginning of melting, although the differences could be negligible. This can be easily visualized in the system $\text{SiO}_2\text{-H}_2\text{O-CO}_2$ using Figure 3. If the quartz apex of the 3-phase triangle dissolves H_2O and/or CO_2 , then the Qz-V leg of the triangle will not rotate parallel to the lines of equal $\text{H}_2\text{O}/\text{CO}_2$ ratios. As an example, the curves presented by Mysen and Boettcher (1975) for the *vapor-saturated solidi* of amphibole-bearing peridotite in the presence of $\text{H}_2\text{O-CO}_2$ vapor are strictly valid only for a specific value of $\text{H}_2\text{O} + \text{CO}_2$. Although, in this case, the effect of small changes in the proportion of total volatile components is small, it would be significant for systems with large proportions of hydrous or carbonate minerals.

Experimentally, there are two ways to lower $\mu_{\text{H}_2\text{O}}$ below that for a nearly pure H_2O vapor. One, already discussed, is to add another component, such as CO_2 , to the vapor. Another is to add a smaller proportion of H_2O than is necessary to saturate the system and produce all of the potential hydrous solid and/or fluid phases. Figure

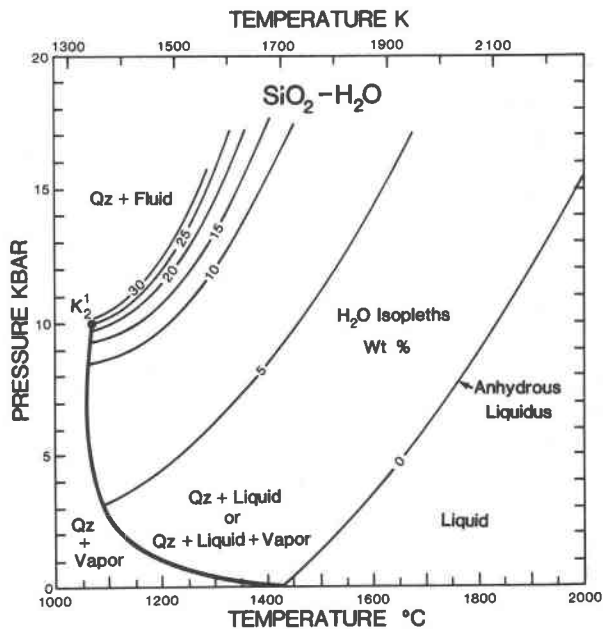


Fig. 4. Pressure-temperature projection, partly schematic, of the *vapor-saturated solidus* for Qz-H₂O and the *liquidus* for various H₂O contents (wt.%) in the system SiO₂-H₂O. The H₂O contents along the *vapor-saturated solidus* are from Kennedy et al. (1962). The anhydrous *liquidus* is from Jackson (1976). Other data are listed in Table 1. At low pressures, quartz is metastable with respect to tridymite or cristobalite.

4 shows such a situation for the system $\text{SiO}_2\text{-H}_2\text{O}$. For example, $\text{SiO}_2 + 5$ wt.% H_2O reacts completely to liquid along the *vapor-saturated solidus* up to about 3 kbar. At higher pressures, there is insufficient H_2O to saturate the liquid, and Qz + L coexist isobarically through a temperature interval up to the 5% isopleth, the *liquidus* for that composition. At pressures above that of the critical end-point K_2^1 , there is no distinction between liquid and vapor, and quartz coexists with a fluid phase up to the *liquidus* (or *fluidus*) temperature for that particular isopleth and pressure. For example, runs #548 and 549 define the *liquidus* between 15 and 18 wt.% H_2O at 17.0 kbar and 1380°C . These *liquidus* [L(S)] in Figure 4 (wt.%) are analogous to the calculated curves labelled 0.65, 0.6, 0.55, etc. (in mole%) in Figure 2. Also shown in Figure 2 are the isopleths ($X_{\text{H}_2\text{O}}^{\text{V}}$) on the L(V) surface.

It is possible to construct a similar *liquidus* diagram for the system $\text{SiO}_2\text{-H}_2\text{O-CO}_2$, but representation is unwieldy because the *liquidus* are functions of $X_{\text{H}_2\text{O}}^{\text{V}}$ and total volatile content.

Summary

The system $\text{SiO}_2\text{-H}_2\text{O-CO}_2$ is sufficiently compositionally simple to allow investigations of mechanisms that are more complex in other systems, such as those containing feldspar components. The present results reveal that carbon is quite soluble in hydrous-silicate liquids at

pressures above 10–15 kbar, probably dissolving as molecular CO_2 , and possibly as tetrahedral carbon. Phase transformations in the liquids change the trajectories of the melting curves and may result in increased solubility of carbon in the liquid.

This system also serves as a model for understanding the effects of changes in $\mu_{\text{H}_2\text{O}}$, $X_{\text{H}_2\text{O}}^V$, etc. on melting relationships during the generation of magmas.

Acknowledgments

Discussions with Prof. Wayne Dollase and Robert Luth of UCLA have been very helpful. Dave Friedman, Ofra Stauber, Karen McBride, Steve Chambers, Jon Daskin, and Scott Boettcher assisted with maintenance and operation of the high-pressure equipment, and Harriet Arnoff typed the manuscript. Prof. Edward Stolper provided a very useful review. The National Science Foundation supported this research with Grants EAR78-16413, EAR82-10695, and EAR83-06410.

References

- Boettcher, A. L. and Wyllie, P. J. (1969) The system $\text{CaO-SiO}_2\text{-CO}_2\text{-H}_2\text{O}$ —III. Second critical end-point on the melting curve. *Geochimica et Cosmochimica Acta*, 33, 611–632.
- Boettcher, A., Guo, Q., and Bohlen, S. R. (1982b) Melting and liquid structure of feldspars. *EOS*, 63, 1136.
- Boettcher, A. L., Mysen, B. O., and Allen, J. C. (1973) Techniques for the control of water fugacity for experimentation in solid-media high-pressure apparatus. *Journal of Geophysical Research*, 78, 5898–5901.
- Boettcher, A. L., Burnham, C. Wayne, Windom, K. E., and Bohlen, S. R. (1982a) Liquids, glasses, and the melting of silicates to high pressures. *Journal of Geology*, 90, 127–138.
- Boettcher, A. L., Windom, K. E., Bohlen, S. R., and Luth, R. W. (1981) Low-friction, anhydrous, low- to high-temperature furnace sample assembly for piston-cylinder apparatus. *Reviews of Scientific Instruments*, 52, 1903–1904.
- Bohlen, S. and Boettcher, A. L. (1982) The quartz \rightleftharpoons coesite transformation: a precise determination and the effects of other components. *Journal of Geophysical Research*, 87, 7073–7078.
- Bohlen, S. R., Boettcher, A. L., and Wall, V. J. (1982) The system albite- $\text{H}_2\text{O-CO}_2$: a model for melting and activities of water at high pressures. *American Mineralogist*, 67, 451–462.
- Bohlen, S. R., Essene, E. J., and Boettcher, A. L. (1980b) Reinvestigation and application of olivine-quartz-orthopyroxene barometry. *Earth and Planetary Science Letters*, 47, 1–10.
- Bohlen, S. R., Wall, V. J., and Boettcher, A. L. (1983) Geobarometry in granulites. In S. K. Saxena, Ed., *Advances in Physical Geochemistry*, p. 141–171. Springer-Verlag, New York.
- Bohlen, S. R., Boettcher, A. L., Dollase, W. A., and Essene, E. J. (1980a) The effect of manganese on olivine-quartz-orthopyroxene stability. *Earth and Planetary Science Letters*, 47, 11–20.
- Brown, I. D. and Shannon, R. D. (1973) Empirical bond-strength-bond-length curves for oxides. *Acta Crystallographica*, A29, 266–282.
- Burnham, C. Wayne (1979) The importance of volatile constituents. In H. S. Yoder, Jr., Ed., *The Evolution of the Igneous Rocks*, p. 439–482. Princeton University Press, New Jersey.
- Burnham, C. Wayne (1981) The nature of multicomponent aluminosilicate melts. In D. T. Rickard and F. E. Wickman, Eds., *Chemistry and Geochemistry at High Temperatures and Pressures*, p. 197–229. Pergamon Press, New York.
- Cohen, L. H. and Klement, W., Jr., (1967) High-low quartz inversion: Determination to 35 kilobars. *Journal of Geophysical Research*, 72, 4245–4251.
- Eggler, D. H. and Kadik, A. A. (1979) The system $\text{NaAlSi}_3\text{O}_8\text{-H}_2\text{O-CO}_2$ to 20 kbar pressure: I. Compositional and thermodynamic relations of liquids and vapors coexisting with albite. *American Mineralogist*, 64, 1036–1048.
- Fine, G. and Stolper, E. (1983) The speciation of carbon dioxide in silicate glasses. *EOS*, 64, 875.
- Greig, J. W. (1927) Immiscibility in silicate melts. *American Journal of Science*, 13, 1–44.
- Greig, J. W. (1954) *Carnegie Institution of Washington Yearbook*, 54, 129–134.
- Holloway, J. R. (1977) Fugacity and activity of molecular species in supercritical fluids. In D. G. Fraser, Ed., *Thermodynamics of Geology*, p. 161–181. Reidel, Dordrecht, The Netherlands.
- Jackson, I. (1976) Melting of the silica isotopes SiO_2 , BeF_2 and GeO_2 at elevated pressures. *Physics of the Earth and Planetary Interiors*, 13, 218–231.
- Kennedy, G. C., Wasserburg, G. J., Heard, H. C., and Newton, R. C. (1962) The upper three-phase region in the system $\text{SiO}_2\text{-H}_2\text{O}$. *American Journal of Science*, 260, 501–521.
- Kerrick, D. M. and Jacobs, G. K. (1981) A modified Redlich-Kwong equation for H_2O , CO_2 , and $\text{H}_2\text{O-CO}_2$ mixtures at elevated temperatures and pressures. *American Journal of Science*, 281, 735–767.
- Klement, W., Jr. and Cohen, L. H. (1968) High-low quartz inversion: thermodynamics of the Lambda Transition. *Journal of Geophysical Research*, 73, 2249–2259.
- Klement, W., Jr. and Jayaraman, A. (1966) Phase relations and structures of solids at high pressures. *Progress in Solid State Chemistry*, 3, 289–374.
- MacKenzie, J. D. (1960) Fusion of quartz and cristobalite. *Journal of the American Ceramic Society*, 43, 615–620.
- Mysen, B. O. and Boettcher, A. L. (1975) Melting of a hydrous mantle: I. Phase relations of natural peridotite at high pressures and temperatures with controlled activities of water, carbon dioxide, and hydrogen. *Journal of Petrology*, 16, 520–548.
- Mysen, B. O. and Virgo, D. (1980) Solubility mechanisms of carbon dioxide in silicate melts: a Raman spectroscopic study. *American Mineralogist*, 65, 885–899.
- Mysen, B. O., Eggler, D. H., Seitz, M. G., and Holloway, J. R. (1976) Carbon dioxide in silicate melts and crystals. Part I. Solubility measurements. *American Journal of Science*, 276, 455–479.
- Nakamura, Y. (1974) The system $\text{SiO}_2\text{-H}_2\text{O-H}_2$ at 15 Kbar. *Carnegie Institution of Washington Yearbook*, 73, 259–263.
- Ostrovskii, I. A., Mishina, G. P., and Povilaitis, V. M. (1959) Pressure-temperature projection of the system silica-water. *Doklady Akademii Nauk SSSR (Doklady Academy of Sciences USSR)*, 126, 587–588.
- Richet, P., Bottinga, Y., Denielou, L., Petitot, J. P., and Tequi, C. (1982) Thermodynamic properties of quartz, cristobalite and amorphous SiO_2 : drop calorimetry measurements between 1000 and 1800 K and a review from 0 to 2000 K. *Geochimica et Cosmochimica Acta*, 46, 2639–2658.
- Shettel, D. L. (1973) Solubility of quartz in $\text{H}_2\text{O-CO}_2$ fluids at 5 kb and 500–900°C. *EOS*, 54, 480.

- Stewart, D. B. (1967) Four-phase curve in the system $\text{CaAl}_2\text{-Si}_2\text{O}_8\text{-SiO}_2\text{-H}_2\text{O}$ between 1 and 10 kilobars. *Schweizerische Mineralogische und Petrographische Mitteilungen*, 47/1, 35–59.
- Stolper, E. (1982) The speciation of water in silicate melts. *Geochimica et Cosmochimica Acta*, 46, 2609–2620.
- Wyllie, P. J. (1962) The petrogenetic model, an extension of Bowen's petrogenetic grid. *Geological Magazine*, 99, 558–569.
- Wyllie, P. J. (1979) Magmas and volatile components. *American Mineralogist*, 64, 469–500.
- Wyllie, P. J. and Tuttle, O. F. (1960) Experimental investigation of silicate systems containing two volatile components. Part I. Geometrical considerations. *American Journal of Science*, 258, 498–517.

*Manuscript received, August 10, 1983;
accepted for publication, April 6, 1984.*